Published in final edited form as:
Clin Cancer Res. 2014 July 15; 20(14): 3721–3729. doi:10.1158/1078-0432.CCR-13-3405.

A High Affinity, High Stability Photoacoustic Agent for Imaging Gastrin Releasing Peptide Receptor in Prostate Cancer

Jelena Levi[1,2], **Ataya Sathirachinda**[1,2], and **Sanjiv Sam Gambhir**[1,2,*]

[1]Canary Center at Stanford for Cancer Early Detection, Palo Alto

[2]Molecular Imaging Program at Stanford, Department of Radiology and Bio-X Program, Stanford University, Palo Alto

Abstract

Purpose—To evaluate the utility of targeted photoacoustic imaging in providing molecular information to complement intrinsic functional and anatomical details of the vasculature within prostate lesion.

Experimental Design—We developed a photoacoustic imaging agent, AA3G-740, that targets gastrin releasing peptide receptor (GRPR), found to be highly overexpressed in prostate cancer. The binding specificity of the agent was evaluated in human prostate cancer cell lines PC3 and LNCaP, and antagonist properties determined by cell internalization and intracellular calcium mobilization studies. The imaging sensitivity was assessed for the agent itself and for the PC3 cells labeled with agent. The in vivo stability of the agent was determined in human plasma and in the blood of living mice. The in vivo binding of the agent was evaluated in PC3 prostate tumor models in mice, and was validated ex vivo by optical imaging.

Results—AA3G-740 demonstrated strong and specific binding to GRPR. The sensitivity of detection in vitro indicated suitability of the agent to image very small lesions. In mice, the agent was able to bind to GRPR even in poorly vascularized tumors leading to nearly 2 fold difference in photoacoustic signal relative to the control agent.

Conclusions—The ability to image both vasculature and molecular profile outside the blood vessels gives molecular photoacoustic imaging a unique advantage over currently employed imaging techniques. The imaging method presented here can find application both in diagnosis and in image guided biopsy.

Keywords

Photoacoustic Molecular Imaging; Prostate cancer; Gastrin releasing peptide recrptor

Introduction

Clinical diagnosis of prostate cancer is made upon histological examination of the tissue obtained by biopsy, indicated for patients with abnormal prostate specific antigen (PSA)

Corresponding Author: Sanjiv Sam Gambhir, Molecular Imaging Program at Stanford, James H. Clark Center, 318 Campus Drive, Stanford, CA 94305-5427 sgambhir@stanford.edu.

levels or rectal examination (1). The biopsy is not lesion directed as the imaging technique currently used to guide the procedure, transrectal ultrasound (TRUS), lacks the specificity to identify the malignancies and is used only to provide anatomical references within prostate. Although imaging plays an important role in all aspects of prostate cancer patient management, from diagnosis to treatment, currently no modality serves as a diagnostic tool. As articulated by the experts in the field, to allow more accurate characterization of the disease an imaging modality should ideally be able to provide anatomical, functional and molecular information (2, 3). Photoacoustic imaging (PAI), a technique closely related to ultrasound, may be able to impart just such fusion of information by imaging vasculature as well as molecular signatures of prostate cancer (4). As a potential clinical tool in management of prostate cancer, PAI has been investigated in small animals as a modality that would enable better localization and detection based on the increased vascularization (5–7) and hypoxia (8) in tumors. A few targeted nanoparticle based molecular imaging agents have been reported but they have not been tested in vivo (9, 10). In this study we develop a photoacoustic imaging agent that binds to gastrin releasing peptide receptor (GRPR) with high affinity and specificity and as such supplies molecular information that complements intrinsic functional and anatomical details provided by endogenous absorbers, hemoglobin and deoxyhemoglobin. The ability to image both vasculature and molecular profile outside the blood vessels gives PAI a unique advantage over currently one of the most promising imaging techniques, TRUS that utilizes microbubble contrast agents (11). Although targeted microbubbles do offer molecular information, because of their large size they are capable of imaging targets found only on or in the blood vessels. Another technique that is showing great promise for improved prostate cancer diagnosis as it can provide both anatomic and functional information is multiparametric magnetic resonance imaging (mpMRI) (12, 13). However, compared to photoacoustic imaging, MRI is relatively expensive and is not ideally suited for real-time imaging.

The target of our agent, GRPR, belongs to a family of G coupled protein receptors that control many cell functions such as proliferation, motility and survival and whose dysregulation contributes to tumor progression, angiogenesis and development of metastases (14). Because of its overexpression in prostate cancer, GRPR has attracted great interest as both therapeutic and imaging target for prostate malignancies (15–19). The receptor's natural ligand is a 27 amino acids long gastrin releasing peptide (GRP) that shows great structural and functional similarity to its amphibian counterpart, the bombesin peptide. GRP is recognized as an autocrine growth factor because of the mitogenic effect it causes after binding to its cognate receptor (20). Besides having antiproliferative properties, GRPR antagonists can demonstrate better *in vivo* targeting (21). This is most probably due to the slower dissociation of antagonists from the receptors (22), binding to a higher number of receptors (23, 24) and better *in vivo* stability of the antagonists (21, 23). Because of the antiproliferative properties and potentially preferable targeting in vivo, the antagonist sequence dFQWAVGHStaL-NH_2 was chosen as a binding moiety for our imaging agent. This peptide shows high affinity binding and antagonist activity (25) and its conjugates with a variety of radiometals, ^{111}In, $^{64/67}$Cu and ^{68}Ga, were evaluated in mice (26, 27) and humans (28). In this report, a fluorescent dye, ATTO740, linked to the peptide through a triple glycine linker, served as a photoacoustic signaling moiety.

Materials and methods

General

All Fmoc amino acids and Rink Amide resin were purchased from EMD Millipore. Peptide syntheses were carried out following the standard solid phase Fmoc synthesis. Analysis and purification of the peptides was performed using the Dionex Summit high-performance liquid chromatography (HPLC) system (Dionex Corporation, Sunnyvale, CA) and reverse phase HPLC column Higins Analytical (Higins Analytical, Mountain View, CA) (C18, 4.6 mm × 250 mm). The mobile phase was 0.1% trifluoroacetic acid (TFA) in water (solvent A) and 0.1% TFA in 90 % acetonitrile (CH_3CN) in water (solvent B). Matrix assisted laser desorption/ionization mass spectrometry was performed by the Canary Center proteomics facility on AB Sciex 5800 TOF/TOF System (Foster City, CA). The absorbance measurements were performed using Cary50 (Varian), fluorescence measurements using FluoroMax4 (Horiba).

Dye selection—The dyes, IRDyeQC1 (Li COR, Lincoln, NE), Hilyte750 (Anaspec, Fremont, CA), Alexa750 (Life technologies, Foster City, CA), ATTO740 (ATTO-Tec, Siegen, Germany), RD800 and RD831 (BioVentures Inc., Murfreesboro, TN), ICG (Spectrum chemicals, Gardena, CA) and methylene blue (MB) (emp Biotech GmbH, Berlin, Germany) were dissolved in a minimal amount of dimethylformamide (DMF) and diluted with PBS to a final concentration of 10 μM. Capillary tubes were filled with dye solutions, sealed and embedded in agar phantom. PA signal was determined at maximum absorption wavelength for each dye using the PA instrument described previously (29). For the photobleaching study the dyes were dissolved in a minimal amount of DMF and diluted with PBS to a final concentration of 10 μg/mL concentration, placed in an eppendorf tube and irradiated with laser light using maximum absorption wavelength for 30 minutes. Photobleaching was determined by the change in absorbance after irradiation.

Imaging agent synthesis—Peptides, GGGdFQWAVGHStaL-NH_2 and GGGHdFGWStaAQLV-NH_2 (m/z 1284.6262) were dissolved in phosphate buffered saline (PBS) to afford 1 mg/mL solution. ATTO740 N-hydroxysuccinimide ester (NHS) in DMF (1mg/500uL solution) was added to the peptide solution in 3:1 molar ratio and allowed to react at room temperature for 2 hours. The reaction mixture was injected directly onto the HPLC column, and the separation of the product mixture followed using absorbance at 740 nm. The imaging agents had a retention time of 22.9 minutes and m/z of 1732.4717.

Cell Binding Studies—Human prostate cancer cell lines, PC3 and LNCaP were obtained from American Type Culture Collection and were grown according to the supplier's instructions. Cells (3×10^5) were incubated with 3 pmoles AA3G-740 or CAA3G-740 in PBS for 15 min at 4 °C. Specificity of the binding was determined by incubating PC3 cells with 3 pmoles of AA3G-740 and varying amount of bombesin (1.5×10^{-11}, 1.5×10^{-10}, 1.5×10^{-9}, 1.5×10^{-8} moles). All samples were done in triplicates.

Cell Internalization Studies—PC3 cells (0.5 million) were incubated with 1.5 nmol AA3G-740 in PBSA (PBS containing 1% bovine serum albumin) for 30 and 60 minutes at

37 °C. The same cellular uptake study was performed after 30 minute pre-incubation with 0.5 % sodium azide. The cells were washed three times with cold PBSA and the cell fluorescence analyzed using the Becton Dickinson FACS Aria III instrument. All samples were done in triplicates.

Intracellular Calcium Mobilization—Intracellular Calcium was detected using Fluo-4 NW Calcium Assay kit (Life Technologies) per manufacturer's instructions. PC3 cells (35×10^3) were seeded in a 96 well plate one day ahead of the experiment. Each well was loaded with 100 μL Fluo-4 dye in assay buffer and incubated for 30 minutes at 37 °C, followed by 30 minutes incubation at room temperature. The cell fluorescence (494 excitation/516 nm emission) was determined before and 30 minutes after the addition of AA3G-740 (1, 2.5, 10 and 25 nmol) using Tecan Infinite M 1000 microplate reader. To serve as a positive reference, cells were incubated with 25 nmol ionomycin (MP Biomedicals, Santa Ana, CA). All samples were done in triplicates.

Sensitivity study—Solutions containing different amounts (50, 100, 250 and 500 pmol) of AA3G-740 agent dissolved in PBS were placed directly in the imaging dimple of the Nexus 128 photoacoustic instrument (Endra Lifesciences) and PA signal detected using 750 nm wavelength. Different number of PC3 cells (0.1, 0.2, 0.5, 1.5 and 3.5 million) were incubated with 2.5 nmol AA3G-740 in PBS for 30 minutes at 37 °C. After washing three times with cold PBS, the cells were suspended in 50 μL PBS and placed directly in the dimple of the PA instrument for determination of photoacoustic signal. All samples were done in triplicates.

Imaging agents' stability and blood metabolism—3 nmol solution of AA3G-740 and CAA3G-740 in PBS were incubated in 500 μL pooled male human plasma (Innovative research) for 30 and 60 minutes. After addition of 1mL acetonitrile, plasma proteins were removed by centrifugation and supernatant injected directly onto the HPLC column. The HPLC conditions were the same as for the purification of the imaging agents described above. Similarly, metabolism of AA3G-740 in blood was tested 30 and 60 minutes after injection of the agent using the same HLPC method. All samples were done in triplicates.

Photoacoustic imaging of GRPR in PC3 tumors in mice—All animal studies were performed in accordance with the Guidelines for the Care and Use of Research Animals established by the Stanford University. Eight week old nude male mice (Charles River) were injected with 3 million PC3 cells into the rear leg flank. Mice bearing 0.5–0.7 cm PC3 tumors (n=6 for AA3G-740, n=4 for CAA3G-740) were photoacoustically imaged using a commercial photoacoustic computed tomography system (30, 31) (Nexus 128, Endra Inc.). The system uses a tunable nanosecond pulsed laser (7ns pulses, 20 Hz pulse repetition frequency, about 7mJ/pulse on the animal surface, wavelength range 680 nm to 950 nm) and 128 unfocused ultrasound transducers (with 5 MHz center frequency and 3 mm diameter) arranged in a hemi-spherical bowl filled with water. We used 750 nm light with 100 views and 100 pulses/view. For each animal we first obtained pre-injection data at 750 nm. The imaging agent (10 nmol) was dissolved in 200 μL PBS (pH 7.4) and administered to mice via tail-vein injection. The data was acquired 30 and 60 minutes after the injection of the

imaging agent The agent was dissolved in PBS Volume rendered three dimensional (3D) photoacoustic images are reconstructed off-line using data acquired from all 128 transducers from all views using a filtered back-projection algorithm. The algorithm corrects for pulse to pulse variations in the laser intensity and small changes in the temperature that effect acoustic velocity in the water. The reconstructed 3D raw data is then analyzed using AMIDE software (32).

Ex vivo Studies—Mice were sacrificed 30 and 60 minutes postinjection of 10 nmol AA3G-740 (n=3 for each time point). Optical imaging of the excised organs was carried out using an IVIS200 system (Caliper Life Sciences, Alameda, CA) and ICG filter set. The exposure time for images was 10 s. Quantitative analysis was performed using the Living Image® 4.0 software.

Results

To select a signaling molecule to be conjugated to the GRPR binding peptide that will allow high sensitivity detection we compared the intensity of the photoacoustic signal of the dyes absorbing in the near infrared region, focusing on the longer wavelengths cca. 750 nm, where the background signal is minimal and the intensity of the laser light at its maximum. As a comparison we also evaluated two FDA approved dyes, methylene blue (MB) and indocyanine green (ICG) that are frequently used in photoacoustic studies. Four dyes, IRDyeQC-1, ATTO740, RD-831 and ICG, showed high photoacoustic signal (Figure 1A) but because ATTO740 demonstrated superior photostability (Figure 1B and supplementary information) it was selected as the most suitable signaling moiety for our imaging agent. The dye was conjugated to the targeting peptide through a triple glycine linker that was shown to allow retention of the peptide's binding affinity (33, 34). The targeting peptide was a D-Phe^{6}-bombesin[6–14] with modifications at positions 13 and 14 that impart antagonist properties, high binding and stability toward peptidases (Figure 1C). The control agent, CAA3G-740, contained the same linker and dye but a scrambled peptide, HdFGWStaAQLV-NH_2. Besides photoacoustic, ATTO 740 shows a fluorescent signal (Figure 1D) as well that enables bimodal imaging and efficient binding characterization in cell culture by FACS. Spectral characterization of the conjugate indicated 750 nm to be the wavelength with maximum photoacoustic signal.

The binding of the agents was tested in two prostate cancer cell lines with relatively low and high level of GRPR expression, LNCaP and PC3 (19, 35). The GRPR specificity of AA3G-740 was demonstrated by the intense labeling of PC3 cells that was efficiently blocked in the presence of bombesin in a dose dependent manner (Figure 2A and supplementary information). Conversely, LNCaP cells that have lower levels of GRPR showed minimal binding of AA3G-740 (Figure 2B). Control agent, CAA3G-740 did not show appreciable binding to PC3 cells (Figure 2C).

As agonists and antagonists demonstrate different behavior after binding to the receptor, we investigated functional properties of AA3G-740 by evaluating the extent of its internalization and the effect that the binding to GRPR has on intracellular calcium mobilization (Figure 3). While agonists show fast and massive internalization of the ligand-

receptor complex and cause calcium mobilization, antagonists are largely cell surface bound and do not effect calcium signaling. Both studies indicated that AA3G-740 has antagonistic properties. The amount of the agent that was bound to the cell surface exceeded the internalized portion at both time points tested. Similarly to Demobesin 1, a well investigated GRPR antagonist, the surface bound AA3G-740 reached a plateau at 30 minutes while the internalized portion continued to rise over time (21). Calcium mobilization assay further supported the antagonistic function of AA3G-740 as there was no increase in intracellular calcium even at high doses of the agent. The slight decrease in fluorescence after the addition of the agent at high doses could be explained by the intracellular, intramolecular quenching between the dye used for calcium sensing and ATTO 740.

The sensitivity of detection was determined for the agent itself and for the cells that have been labeled with the agent (Figure 4). We could detect as low as 100 pmol AA3G-740 with linear dependence of the photoacoustic signal on the concentration of the agent. The sensitivity of 100 pmol represents only 1% of the commonly used 10 nmol imaging dose, suggesting aptness for in vivo imaging. The smallest number of AA3G-740 labeled PC3 cells that demonstrated photoacoustic signal significantly higher than the background was found to be 0.5 million. Considering that there are around 10^8 cells in 1 cm^3 tumor (36), the determined cell sensitivity indicates that the agent has the potential to detect very small lesions.

The stability of the agent was determined in human male plasma as well as in blood of living mice (Figure 5). The agent was highly stable in human serum, as only parent compound was observed by HPLC, without detectable decomposition occurring during the 1 hour of incubation. In living mice as well, the major peak observed in blood at 30 minutes post injection was of the parent AA3G-740 agent. The indication of a possible adduct formation was apparent in the existence of small peaks with longer retention times (Figure 5B). At one hour post injection, the intact agent was still the major component but its low level indicated a short blood lifetime (supplementary information).

The efficacy of the agent to bind to and detect GRPR in vivo was evaluated in prostate cancer xenografts implanted in nude mice (Figure 6). Mice bearing PC3 tumors were injected with 10 nmol AA3G-740 or CAA3G-740 and imaged at 30 and 60 minutes post injection. High photoacoustic signal was detected at both time points in mice injected with AA3G-740, while CAA3G-740 administration resulted in a signal barely exceeding the intensity of the pre-injection background. Different accumulation of the agents was confirmed ex vivo by optical imaging (Figure 6b).

Accumulation of the agent in various organs was determined ex vivo by optical imaging (Figure7). The highest signal was observed in gallbladder and liver, followed by intestine kidneys and spleen.

Discussion

Prostate cancer diagnosis and detection can be greatly improved by utilization of an imaging modality that allows better characterization of the disease through describing both functional

and molecular status in the detected lesion. In this study we develop a molecular agent for photoacoustic imaging that can complement intrinsically present signal of blood vessels.

The agent, AA3G-740, was designed to target GRPR receptors found to be overexpressed in prostate cancer. The antagonist GRPR peptide, dFQWAVGHStaL-NH_2, was labeled via a triple glycine linker to the ATTO-740 dye, that showed high photoacoustic signal and good photostability. The specificity of AA3G-740 for GRPR was demonstrated in GRPR highly expressing PC3 cells by the ability of bombesin to prevent binding of the agent to the cells. Low expressing LNCaP cells showed minimal binding of the agent.

The conjugation of the dye was not found to change the functional properties of the antagonist peptide as the binding of the conjugate did not lead to fast internalization, expected from an agonist. In addition, binding of the agent did not seem to have any effect on the calcium signaling in cells. It was first shown for somatostatin and later for GRPR receptors that antagonists, although internalized at a much lower extent than agonists, demonstrate preferable in vivo tumor targeting properties, possibly due to strong, high efficiency labeling. Besides for these important in vivo characteristics, it was essential to confirm the antagonist function of our imaging agent because of the dose of the agent needed for photoacoustic and optical imaging. While agonists have mitogenic properties, antagonists have been proposed as anticancer agents that have shown no toxicity in clinical trials at high doses (37) and are as such suitable as agents requiring more than tracer level for imaging.

The sensitivity of AA3G-740 in vitro was found to be sufficient to detect as low as 1% of the commonly used 10 nmol imaging dose and to allow imaging of as little as 0.5 million cells. Such excellent sensitivity is particularly important in view of the size of the signaling moiety used in the agent. Most of the agents developed for photoacoustic imaging are nanoparticles that have masses several orders of magnitude higher than ATTO-740. Found high sensitivity suggests that on a mass level ATTO-740 provides a more intense photoacoustic signal than most nanoparticles, and as such is more likely to have a better safety profile for in vivo applications.

A recent study described rapid metabolism of ^{68}Ga labeled bombesin antagonist in blood of healthy volunteers that resulted in more than 50 % agent decomposition at only 20 minutes postinjection (28). Although AA3G-740 contains the same antagonist peptide, we did not observe any decomposition during one hour incubation in human male plasma. The difference in stability between ^{68}Ga and ATTO740 labeled GRPR antagonist can be explained by differences in size, charge or hydrophobicity that lead to differential susceptibility to proteolysis. In blood of mice, at 30 minutes postinjection, the major peak was of the parent AA3G-740 with no indication of proteolysis. The other peaks that were observed in HPLC chromatogram had longer retention times indicating possible adducts with molecules from the blood. Short blood lifetime, expected from an agent of this size, was evident from a low level of AA3G-740 present in blood at 60 minutes postinjection.

Considering the blood lifetime we evaluated in vivo targeting of AA3G-740 and CAA3G-740 at 30 and 60 minutes post injection in tumor bearing mice (Figure 6). As a

blocking study would require potentially a lethal dose of bombesin, the specificity of the binding was established through the use of the control agent designed not to bind to GRPR. At both time points there was a clear distinction between the two agents. While binding of AA3G-740 led to an intense photoacoustic signal, close to 2 fold higher than the background, the injection of the control agent increased minimally over time. In addition, the signal in tumors of mice injected with the control agent decreased over time, suggesting that the signal observed at 30 minutes p.i. was most likely due to the agent present in the vasculature (Figure 6C).

The images in Figure 6 clearly illustrate the importance of having molecular information in addition to the blood vessel network status. The pre-injection photoacoustic signals that correspond to tumor vasculature were noticeably different in two PC3 tumors presented in the figure, suggestive of their low and high vascularization state. Nonetheless, the active agent was able to reveal the GRPR status of the tumor despite its poor vascularization, while the inability of CAA3G-740 to bind to the receptor led to minimal photoacoustic signal in a richly vascular lesion. Besides indicating the specificity of AA3G-740, these results suggest that molecular information unrelated to vascularization can be a differentiating point for benign and malignant prostate lesions with similar vascular status.

Optical ex vivo imaging of the major organs at 1 hour p.i. indicated hepatobilliary excretion as gallbladder, liver and intestine displayed the highest photoacoustic signal. Similar clearance route was observed for some of the other GRPR antagonist agents (18, 26, 38).

There are several issues that need to be addressed in the future studies. The AA3G-740 was evaluated in mice at only two time points due to its short blood lifetime. Although we found 30 minutes post injection to be a sufficient time to allow specific binding of the agent, for a potential clinical translation it would be beneficial to extend the blood lifetime and re-determine the optimal imaging time. As the lifetime greatly depends on the size of the agent, we will explore pegylation as a means to increase the size and improve pharmacokinetics of the agent. In addition, as linkers seem to play an important role for tumor targeting we will investigate amino acids with different size and charge to optimize the targeting efficiency of the agent (18). Lastly, it will be important to determine the targeting ability of the agent in other prostate tumor models such as orthotropic, androgen dependent and independent.

This is the first report of molecular PAI of prostate cancer in small animals. As exemplified by the presented data, PAI using GRPR specific agent afforded visualization of the molecular profile of the tumors with relatively high resolution and specificity. The imaging method presented here can find application in diagnosis as well as in image guided biopsy. One of the most pressing issues in prostate cancer are overdiagnosis and overtreatment, caused by our current inability to differentiate between an aggressive and an indolent disease. The differentiation between the low and high risk tumors could be enabled by the use of agents, similar to the one presented here, that target the molecular differences between the lesions. Prostate imaging using PAI has a great potential for clinical translation and this study warrants further investigations in that direction.

Supplementary Material

Refer to Web version on PubMed Central for supplementary material.

Acknowledgments

Financial Support: This work was supported in part by National Institutes of Health Grants NCI ICMIC P50 CA114747 (SSG), CCNE U54 CA119367 (SSG), and the Canary Foundation (SSG).

References

1. http://www.uptodate.com/contents/clinical-presentation-and-diagnosis-of-prostate-cancer.
2. Kelloff GJ, Choyke P, Coffey DS. Challenges in clinical prostate cancer: role of imaging. AJR Am J Roentgenol. 2009; 192:1455–1470. [PubMed: 19457806]
3. Hricak H, Choyke PL, Eberhardt SC, Leibel SA, Scardino PT. Imaging prostate cancer: a multidisciplinary perspective. Radiology. 2007; 243:28–53. [PubMed: 17392247]
4. Wang LV, Hu S. Photoacoustic tomography: in vivo imaging from organelles to organs. Science. 2012; 335:1458–1462. [PubMed: 22442475]
5. Bauer DR, Olafsson R, Montilla LG, Witte RS. 3-D photoacoustic and pulse echo imaging of prostate tumor progression in the mouse window chamber. J Biomed Opt. 2011; 16:026012. [PubMed: 21361696]
6. Wang X, Roberts WW, Carson PL, Wood DP, Fowlkes JB. Photoacoustic tomography: a potential new tool for prostate cancer. Biomed Opt Express. 2010; 1:1117–1126. [PubMed: 21258534]
7. Olafsson R, Bauer DR, Montilla LG, Witte RS. Real-time, contrast enhanced photoacoustic imaging of cancer in a mouse window chamber. Opt Express. 2010; 18:18625–18632. [PubMed: 20940754]
8. Shao Q, Morgounova E, Jiang C, Choi J, Bischof J, Ashkenazi S. In vivo photoacoustic lifetime imaging of tumor hypoxia in small animals. J Biomed Opt. 2013; 18:076019. [PubMed: 23877772]
9. Kim G, Huang SW, Day KC, O'Donnell M, Agayan RR, Day MA, et al. Indocyanine-green-embedded PEBBLEs as a contrast agent for photoacoustic imaging. J Biomed Opt. 2007; 12:044020. [PubMed: 17867824]
10. Agarwal A, Huang SW, O'Donnell M, Day KC, Day M, Kotov N, et al. Targeted gold nanorod contrast agent for prostate cancer detection by photoacoustic imaging. J Appl Phys. 2007; 102
11. Kundavaram CR, Halpern EJ, Trabulsi EJ. Value of contrast-enhanced ultrasonography in prostate cancer. Curr Opin Urol. 2012; 22:303–309. [PubMed: 22617061]
12. Turkbey B, Pinto PA, Choyke PL. Imaging techniques for prostate cancer: implications for focal therapy. Nat Rev Urol. 2009; 6:191–203. [PubMed: 19352394]
13. Gupta RT, Kauffman CR, Polascik TJ, Taneja SS, Rosenkrantz AB. The state of prostate MRI in 2013. Oncology. 2013; 27:262–270. [PubMed: 23781689]
14. Dorsam RT, Gutkind JS. G-protein-coupled receptors and cancer. Nat Rev Cancer. 2007; 7:79–94. [PubMed: 17251915]
15. Mansi R, Fleischmann A, Macke HR, Reubi JC. Targeting GRPR in urological cancers -from basic research to clinical application. Nat Rev Urol. 2013; 10:235–244. [PubMed: 23507930]
16. Cai QY, Yu P, Besch-Williford C, Smith CJ, Sieckman GL, Hoffman TJ, et al. Near-infrared fluorescence imaging of gastrin releasing peptide receptor targeting in prostate cancer lymph node metastases. The Prostate. 2013; 73:842–854. [PubMed: 23280511]
17. Breeman WA, Hofland LJ, de Jong M, Bernard BF, Srinivasan A, Kwekkeboom DJ, et al. Evaluation of radiolabelled bombesin analogues for receptor-targeted scintigraphy and radiotherapy. International journal of cancer Journal international du cancer. 1999; 81:658–665. [PubMed: 10225459]
18. Mu L, Honer M, Becaud J, Martic M, Schubiger PA, Ametamey SM, et al. In vitro and in vivo characterization of novel 18F-labeled bombesin analogues for targeting GRPR-positive tumors. Bioconjugate chemistry. 2010; 21:1864–1871. [PubMed: 20857927]

19. Honer M, Mu L, Stellfeld T, Graham K, Martic M, Fischer CR, et al. 18F-labeled bombesin analog for specific and effective targeting of prostate tumors expressing gastrin-releasing peptide receptors. Journal of nuclear medicine : official publication, Society of Nuclear Medicine. 2011; 52:270–278.
20. Cuttitta F, Carney DN, Mulshine J, Moody TW, Fedorko J, Fischler A, et al. Bombesin-like peptides can function as autocrine growth factors in human small-cell lung cancer. Nature. 1985; 316:823–826. [PubMed: 2993906]
21. Cescato R, Maina T, Nock B, Nikolopoulou A, Charalambidis D, Piccand V, et al. Bombesin receptor antagonists may be preferable to agonists for tumor targeting. Journal of nuclear medicine : official publication, Society of Nuclear Medicine. 2008; 49:318–326.
22. Vauquelin G, Van Liefde I. Slow antagonist dissociation and long-lasting in vivo receptor protection. Trends in pharmacological sciences. 2006; 27:356–359. [PubMed: 16766051]
23. Ginj M, Zhang H, Waser B, Cescato R, Wild D, Wang X, et al. Radiolabeled somatostatin receptor antagonists are preferable to agonists for in vivo peptide receptor targeting of tumors. Proceedings of the National Academy of Sciences of the United States of America. 2006; 103:16436–16441. [PubMed: 17056720]
24. Sleight AJ, Stam NJ, Mutel V, Vanderheyden PM. Radiolabelling of the human 5-HT2A receptor with an agonist, a partial agonist and an antagonist: effects on apparent agonist affinities. Biochemical pharmacology. 1996; 51:71–76. [PubMed: 8534270]
25. Llinares M, Devin C, Chaloin O, Azay J, Noel-Artis AM, Bernad N, et al. Syntheses and biological activities of potent bombesin receptor antagonists. The journal of peptide research : official journal of the American Peptide Society. 1999; 53:275–283. [PubMed: 10231715]
26. Mansi R, Wang X, Forrer F, Waser B, Cescato R, Graham K, et al. Development of a potent DOTA-conjugated bombesin antagonist for targeting GRPr-positive tumours. European journal of nuclear medicine and molecular imaging. 2011; 38:97–107. [PubMed: 20717822]
27. Zhang H, Abiraj K, Thorek DL, Waser B, Smith-Jones PM, Honer M, et al. Evolution of bombesin conjugates for targeted PET imaging of tumors. PloS one. 2012; 7:e44046. [PubMed: 23024746]
28. Roivainen A, Kahkonen E, Luoto P, Borkowski S, Hofmann B, Jambor I, et al. Plasma Pharmacokinetics, Whole-Body Distribution, Metabolism, and Radiation Dosimetry of 68Ga Bombesin Antagonist BAY86-7548 in Healthy Men. Journal of nuclear medicine : official publication, Society of Nuclear Medicine. 2013
29. De la Zerda A, Zavaleta C, Keren S, Vaithilingam S, Bodapati S, Liu Z, et al. Carbon nanotubes as photoacoustic molecular imaging agents in living mice. Nature nanotechnology. 2008; 3:557–562.
30. Bohndiek SE, Bodapati S, Van De Sompel D, Kothapalli SR, Gambhir SS. Development and application of stable phantoms for the evaluation of photoacoustic imaging instruments. PloS one. 2013; 8:e75533. [PubMed: 24086557]
31. Van de Sompel D, Sasportas LS, Dragulescu-Andrasi A, Bohndiek S, Gambhir SS. Improving image quality by accounting for changes in water temperature during a photoacoustic tomography scan. PloS one. 2012; 7:e45337. [PubMed: 23071512]
32. Loening AM, Gambhir SS. AMIDE: a free software tool for multimodality medical image analysis. Mol Imaging. 2003; 2:131–137. [PubMed: 14649056]
33. Kuil J, Velders AH, van Leeuwen FW. Multimodal tumor-targeting peptides functionalized with both a radio- and a fluorescent label. Bioconjugate chemistry. 2010; 21:1709–1719. [PubMed: 20812730]
34. Ma L, Yu P, Veerendra B, Rold TL, Retzloff L, Prasanphanich A, et al. In vitro and in vivo evaluation of Alexa Fluor 680-bombesin[7–14]NH2 peptide conjugate, a high-affinity fluorescent probe with high selectivity for the gastrin-releasing peptide receptor. Molecular imaging. 2007; 6:171–180. [PubMed: 17532883]
35. Aprikian AG, Han K, Chevalier S, Bazinet M, Viallet J. Bombesin specifically induces intracellular calcium mobilization via gastrin-releasing peptide receptors in human prostate cancer cells. Journal of molecular endocrinology. 1996; 16:297–306. [PubMed: 8782088]
36. Tokita K, Katsuno T, Hocart SJ, Coy DH, Llinares M, Martinez J, et al. Molecular basis for selectivity of high affinity peptide antagonists for the gastrin-releasing peptide receptor. The Journal of biological chemistry. 2001; 276:36652–36663. [PubMed: 11463790]

37. Schwartsmann G, DiLeone LP, Horowitz M, Schunemann D, Cancella A, Pereira AS, et al. A phase I trial of the bombesin/gastrin-releasing peptide (BN/GRP) antagonist RC3095 in patients with advanced solid malignancies. Investigational new drugs. 2006; 24:403–412. [PubMed: 16505950]

38. Hohne A, Mu L, Honer M, Schubiger PA, Ametamey SM, Graham K, et al. Synthesis, 18F-labeling, and in vitro and in vivo studies of bombesin peptides modified with silicon-based building blocks. Bioconjugate chemistry. 2008; 19:1871–1879. [PubMed: 18754574]

Statement of translational relevance

Prostate cancer diagnosis is made upon histological examination of the tissue obtained by biopsy, indicated for patients with abnormal prostate specific antigen (PSA) levels or rectal examination. The biopsy is not lesion directed as the imaging technique currently used to guide the procedure, transrectal ultrasound (TRUS), lacks the specificity to identify the malignancies and is used only to provide anatomical references within prostate. Current clinical diagnosis of prostate cancer can be greatly improved by utilization of an imaging modality that allows better characterization of the disease through evaluation of functional and molecular status in a detected lesion. Molecuar photoacoustic imaging, with good depth penetration in combination with high contrast and resolution has a great potential to be clinically utilized for non-invasive, non-ionizing visualization of prostate lesions. The ability to image both vasculature and molecular profile outside the blood vessels gives photoacoustic imaging a unique advantage over currently employed imaging techniques. The imaging method presented here can find clinical application both in diagnosis and in image guided biopsy.

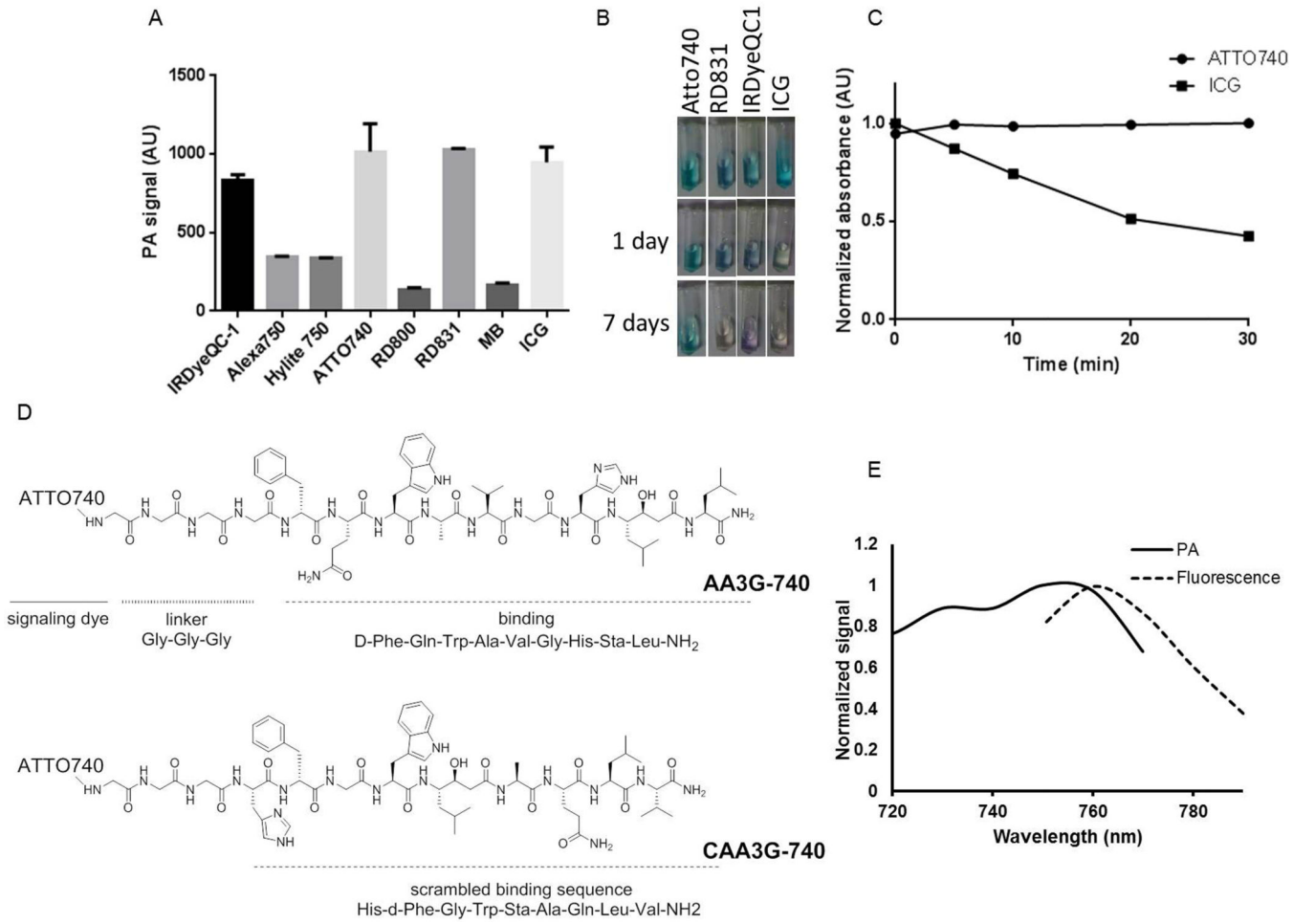

Figure 1. Design and spectral characterization of the GRPR imaging agent

A) The highest photoacoustic signal among the small molecule dyes tested was observed for IRDyeQC-1, ATTO 740, RD831 and ICG. B) Among the dyes that provided a high photoacoustic signal, ATTO-740 showed superior photostability not changing the appearance after being exposed to light for 7 days. C) The absorbance of ATTO740 did not change during a 30 minute irradiation with 740 nm laser light. D) GRPR agent, AA3G-740 consists of antagonist binding moiety, triple glycine linker and ATTO740 as a signaling dye. The control agent, CAA3G-740, has the same signaling dye and linker but a scrambled binding sequence. E) AA3G-740 provides the highest photoacoustic signal at 750 nm and highest fluorescence at 760 nm.

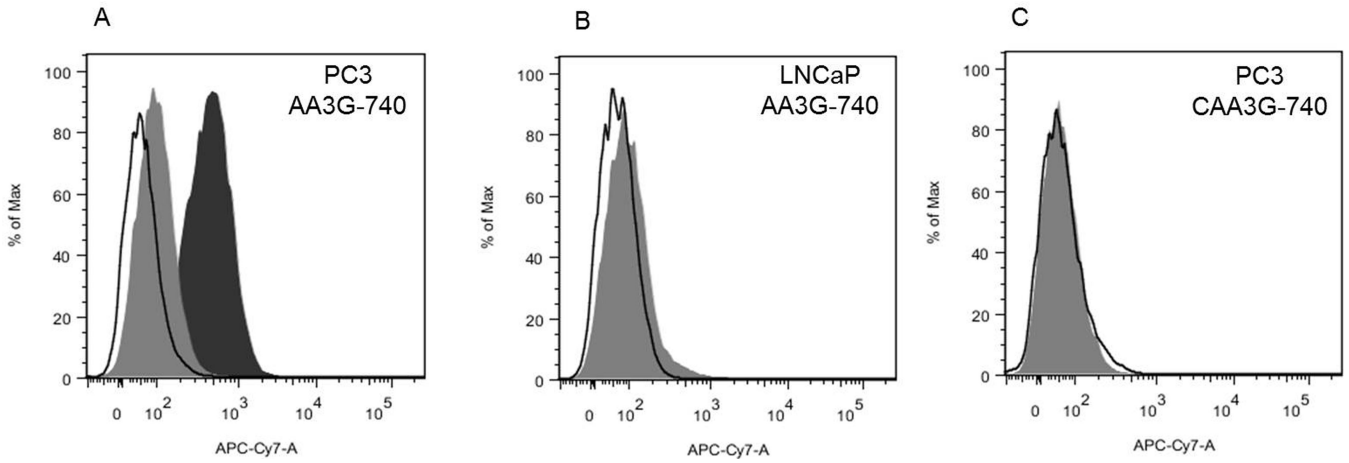

Figure 2. Binding specificity

A) AA3G-740 efficiently labeled PC3 cells that have high level of GRPR (black filled area). Co-incubation with bombesin prevented the binding, resulting in minimal cell fluorescence (gray filled area). B) Low GRPR expressing cells, LNCaP, showed minimal increase in fluorescence (grey filled area). C) Control agent, CAA3G-740 containing a scrambled binding sequence was not able to label PC3 cells (grey filled area). Black outline represent unstained cells in all three panels.

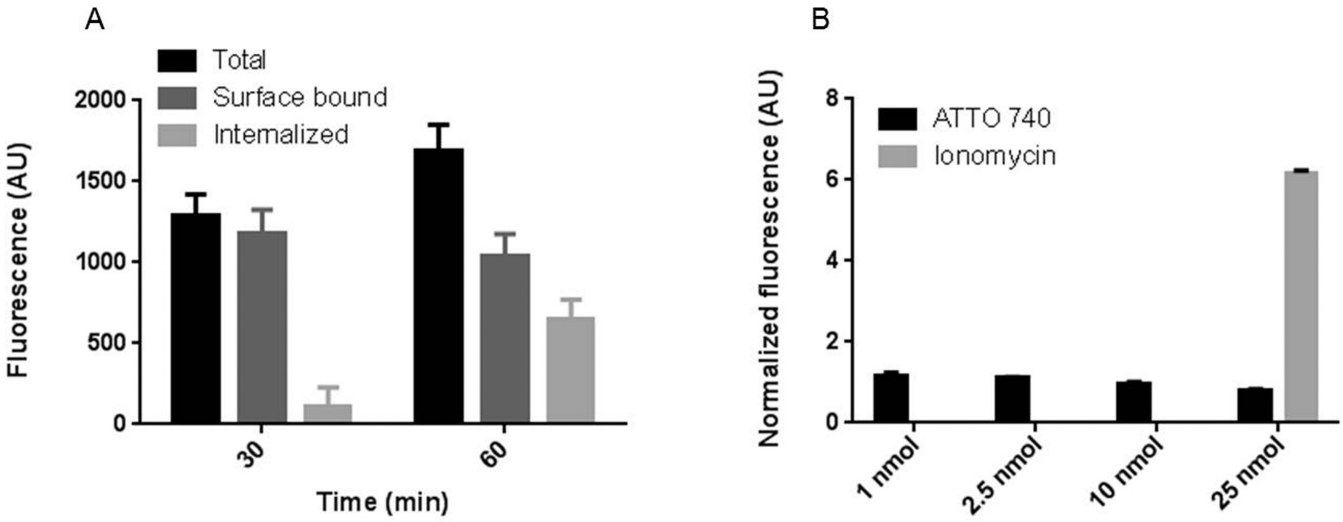

Figure 3. Functional properties of AA3G-740

A) The agent was found to be primarily surface bound. The internalized portion increased over time but it represented a smaller portion of the total amount. B) AA3G-740 binding did not cause calcium internalization at any of the concentrations tested. Both results suggest antagonistic properties of the agent.

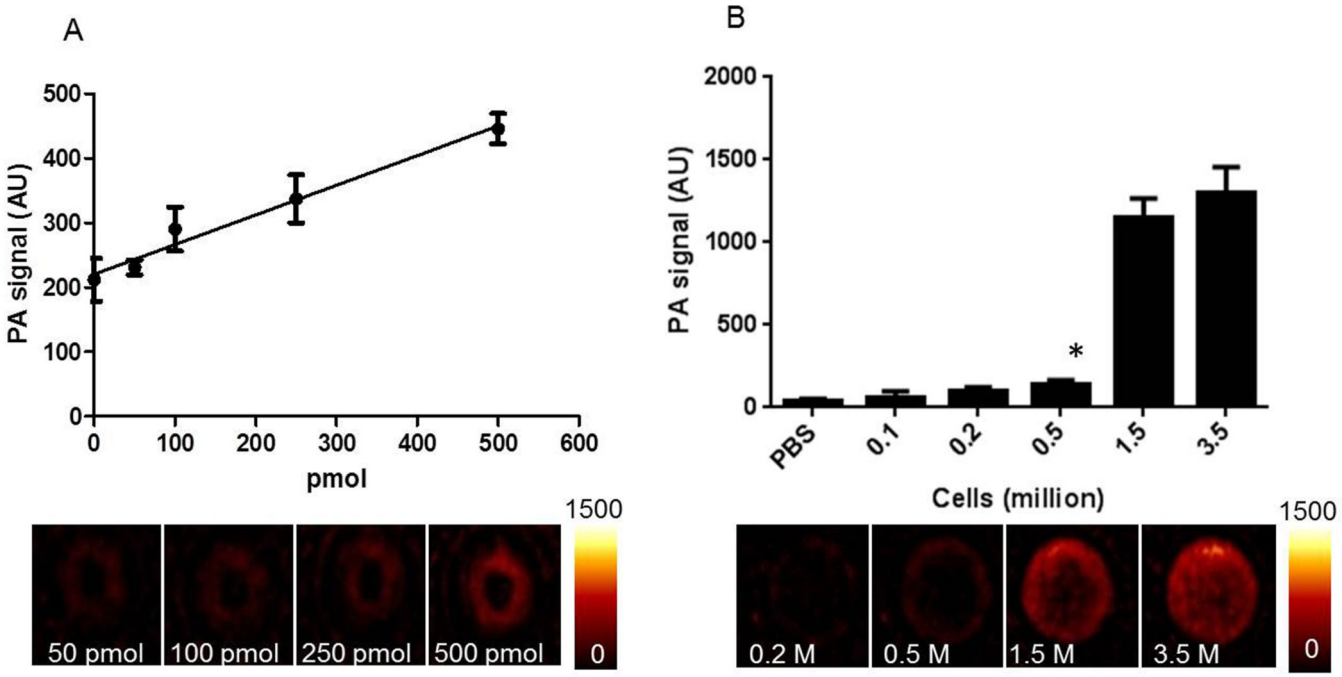

Figure 4. Sensitivity of detection

A) The photoacoustic signal was linearly dependent on the amount of the agent. The lowest amount that could reliably be detected above the background was found to be 100 pmol. B) The lowest detectable number of PC3 cells labeled with AA3G-740 was determined to be 0.5 million.

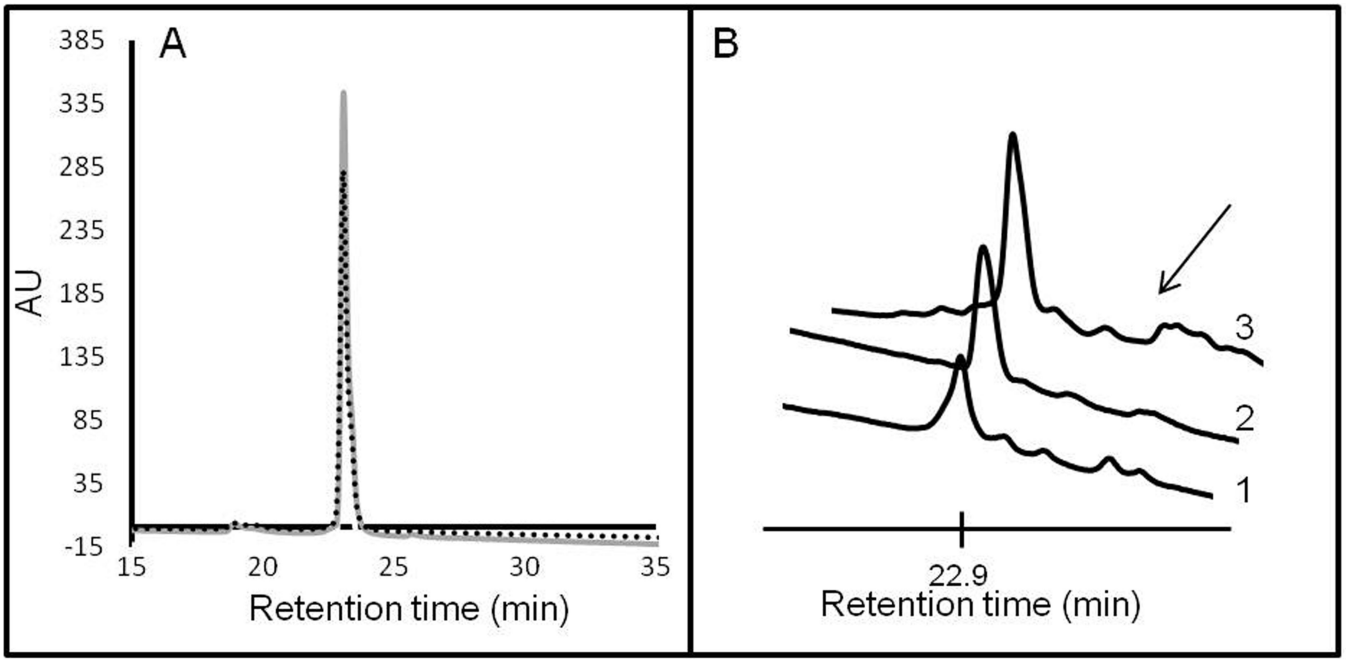

Figure 5. Agent stability

The stability of the agent was determined in human male plasma (A) and in mouse blood (B). There was no evidence of decomposition within one hour of incubation in human plasma (grey line 30 min incubation, dotted line 60 min incubation). In mouse blood, at 30 minutes post injection, the major peak corresponded to the intact agent with minute amount of possible peptide adducts also visible (arrow). The three spectra in B correspond to data from three mice. There was no indication of proteolysis occurring in the blood.

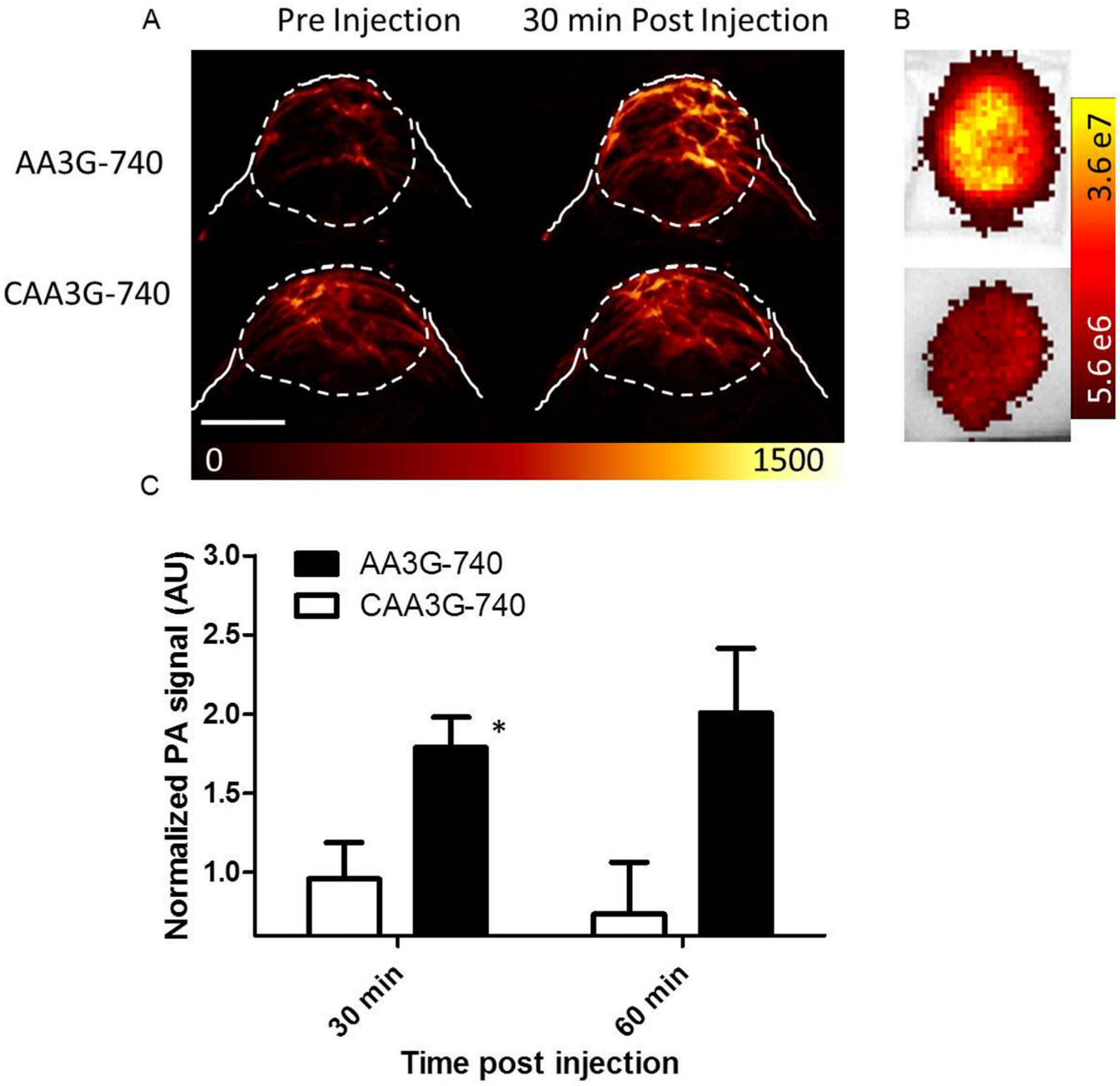

Figure 6. Imaging of GRPR in PC3 tumors

PC3 tumors implanted in nude mice were imaged before and after the injection of 10nmol active or control agent. A) While the injection of AA3G-740 led to close to a 2 fold increase in photoacoustic signal, CAA3G-740 injection caused a minimal change over the background, pre-injection, signal. The scale bar represents 0.5 mm. B) Different accumulation of the two agents was confirmed ex vivo by optical imaging. C) The quantitation of the photoacoustic signals revealed significant difference between tumors injected with the two agents at both time points. The signal in tumors injected with

AA3G-740 (n=6) increased over time, while in the ones injected with CAA3G-740 (n=4) it remained largely constant. The errors bars represent standard deviation. *p<0.05.

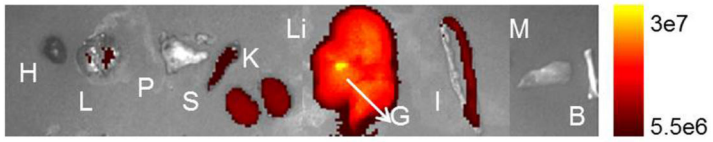

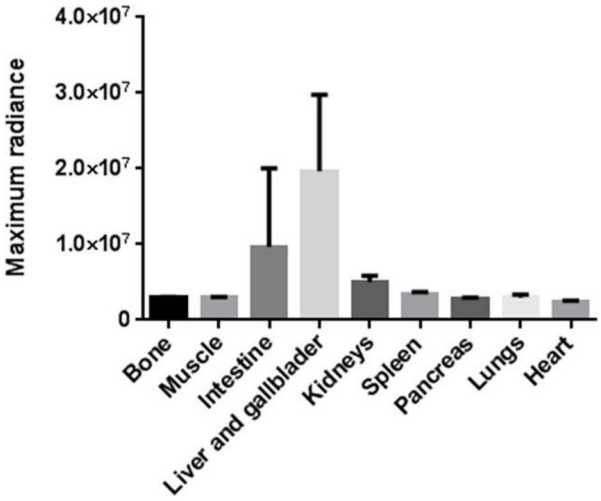

Figure 7. AA3G-740 excretion route

Agent (10 nmol) was injected in mice (n=3) and major organs imaged ex vivo 30 minutes post injection. The highest signal was observed for gallbladder and liver, followed by intestine, kidneys and spleen. H-heart, L- lung, P- pancreas, S-spleen, K- kidneys, Li- liver, G-gallbladder, I-intestine, M-muscle, B-bone.